THE GEOSTATIONARY EARTH RADIATION BUDGET PROJECT

BY J. E. HARRIES, J. E. RUSSELL, J. A. HANAFIN, H. BRINDLEY, J. FUTYAN, J. RUFUS, S. KELLOCK, G. MATTHEWS,* R. WRIGLEY,+ A. LAST, J. MUELLER,# R. MOSSAVATI,# J. ASHMALL,@ E. SAWYER, D. PARKER, M. CALDWELL, P. M. ALLAN, A. SMITH, M. J. BATES, B. COAN, B. C. STEWART, D. R. LEPINE, L. A. CORNWALL, D. R. CORNEY, M. J. RICKETTS, D. DRUMMOND, D. SMART, R. CUTLER, S. DEWITTE, N. CLERBAUX, L. GONZALEZ, A. IPE, C. BERTRAND, A. JOUKOFF, D. CROMMELYNCK, N. NELMS, D. T. LLEWELLYN-JONES, G. BUTCHER, G. L. SMITH, Z. P. SZEWCZYK, P. E. MLYNCZAK, A. SLINGO, R. P. ALLAN, AND M. A. RINGER

A new instrument, GERB, is now operating on the European *Meteosat-8* spacecraft, making unique, accurate, high-time-resolution measurements of the Earth's radiation budget for atmospheric physics and climate studies.

This paper describes a new Earth Radiation Budget (ERB) sensor that is in operation on the first Meteosat Second Generation (MSG) satellite. The Geostationary Earth Radiation Budget (GERB) experiment is providing the first dedicated measurements of the ERB components from geostationary orbit. The paper describes the science background, the instrument and operations, and presents some of the first data. GERB has been performing very successfully since launch.

Anthropogenic changes to our Earth's climate may already be occurring as greenhouse gas concentrations in the atmosphere increase above natural levels, and as the temperature at the Earth's surface shows a significant and rapid rise in the past two decades, compared with the past two millennia (Houghton

AFFILIATIONS: HARRIES, RUSSELL, HANAFIN, BRINDLEY, FUTYAN, RUFUS, KELLOCK, MATTHEWS, WRIGLEY, LAST, MUELLER, MOSSAVATI, AND ASHMALL—Blackett Laboratory, Imperial College, London, United Kingdom; SAWYER, PARKER, CALDWELL, ALLAN, SMITH, BATES, COAN, STEWART, LEPINE, CORNWALL, CORNEY, RICKETTS, DRUMMOND, SMART, AND CUTLER—Rutherford Appleton Laboratory, Oxfordshire, United Kingdom; DEWITTE, CLERBAUX, GONZALEZ, IPE, BERTRAND, JOUKOFF, AND CROMMELYNCK—Royal Meteorological Institute, Brussels, Belgium; NELMS, LLEWELLYN-JONES, AND BUTCHER—University of Leicester, Leicester, United Kingdom; SMITH—National Institute of Aerospace, Hampton, Virginia; SZEWCZYK AND MLYNCZAK—Science Applications International Corporation, Hampton, Virginia; SLINGO AND ALLAN—Environmental Systems Science Centre, University of Reading, Reading, United Kingdom; RINGER—Hadley Centre for Climate Prediction and Research, Met Office, Exeter, United Kingdom
CURRENT AFFILIATIONS: *Analytical Services and Materials, Inc., Hampton, Virginia; +Surface Measurement Systems Ltd., London, United Kingdom; #EUMETSAT, Darmstadt, Germany; @Center for Space Research, Massachusetts Institute of Technology, Cambridge, Massachusetts
CORRESPONDING AUTHOR: J. A. Hanafin, Space and Atmospheric Physics, Imperial College, London SW7 2BZ, United Kingdom
E-mail: j.hanafin@imperial.ac.uk
DOI:10.1175/BAMS-86-7-945

In final form 31 January 2005

et al. 2001; Stott et al. 2000). Ascribing these known changes to specific mechanisms is, however, a very challenging problem, for example, see Allen et al. (2000). Furthermore, the complex feedback processes that can amplify or dampen these increases are not fully understood; among the most important feedbacks are those due to water vapor (e.g., Harries 1997), clouds (e.g., Senior and Mitchell 1993), and aerosol particles (e.g., Charlson et al. 1992). Accurate observations of the system are required to develop and test models and improve their predictions. ERB experiments have proved invaluable in this regard, providing measurements of the reflected sunlight from the Earth and of the thermal IR radiation that is emitted by the planet (e.g. Wielicki et al. 2002). This gives the net top-of-atmosphere (TOA) response of the Earth–atmosphere system to the incoming solar energy (e.g., Gueymard 2004). ERB observations to date have been made from instruments flown in low Earth orbit, which provide good spatial resolution because of the proximity to the surface, but are limited in their temporal sampling. This limits their usefulness for studying events and features such as convective clouds, frontal systems, and aerosol variability from dust storms or from volcanoes.

The aim of the GERB project is to provide the accurate, rapid measurements that are required to study the forcing and feedback mechanisms on the short time scales that are important in many cases, and, in turn, to use improved understanding of these mechanisms to determine interannual and longer-term climate variability. The MSG satellite series is planned to extend over at least a decade, with each satellite carrying a GERB instrument.

A team of European scientists and engineers, led by Imperial College and managed technically by the Rutherford Appleton Laboratory (RAL), has developed this new instrument—the first ever to accurately measure the full spectrum ERB (rather than a series of narrow spectral bands) from geostationary orbit, and its variation with time. Four GERB instruments have been designed and built by RAL, in partnership with European and U.K. institutes and industry, and have been calibrated at Imperial College. The first GERB was launched as an instrument of opportunity on board the *MSG-1* satellite (now renamed *Meteosat-8*) in August 2002. This satellite is currently orbiting above a longitude of 3.5°W, but this may change in the course of the platform lifetime, according to the requirements of the operational mission. It has been operating almost continuously since December 2002, providing near-real-time (NRT) shortwave and longwave TOA radiances and fluxes every 15 min. These are collocated with the data from another instrument on the satellite, the Spinning Enhanced Visible and Infrared Imager (SEVIRI), which is described in more detail in Schmetz et al. (2002) and Munro et al. (2002). SEVIRI is the primary European operational geostationary weather satellite sensor and provides NRT data in 12 narrowband channels every 15 min. *Meteosat-8* is operated by the European Organisation for Exploitation of Meteorological Satellites (EUMETSAT), and will provide over a decade of vital new operational and scientific observations of our Earth.

INSTRUMENT PRINCIPLES AND DESIGN.

The GERB instrument (Harries and Crommelynck 1999; Sandford et al. 2003) consists of two units: the optics unit (shown in Fig. 1), and the electronics unit, both of which are manufactured at RAL. The optics unit (see Fig. 2 for a schematic layout) measures 0.45 m × 0.2 m × 0.2 m and contains the imaging optics and detector system, a despin mirror, and a quartz filter, along with two onboard calibration targets—the thermal blackbody source (BB) and the shortwave calibration monitor (Table 1). The electronics unit controls the instrument and provides data handling.

The overall design specifications for GERB are given in Table 2. These parameters represent the design aims of the instrument. The absolute radiometric and the spatial coregistration accuracies are currently being established in validation activities.

Because the 3-m-diameter satellite platform spins at 100 rpm, the despin mirror is key in GERB's sam-

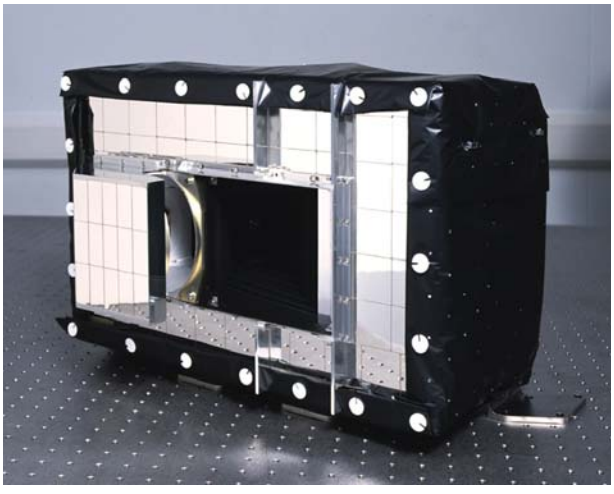

Fig. 1. Photograph of a GERB optics unit, showing the reflective outer coating, the Earth-viewing port in the center, and the SW calibration monitor port to the left.

pling procedure. It counteracts the spacecraft rotation by spinning in the opposite direction, directing a shuttered "frozen" beam of incoming radiation, via the telescope optics, onto the detector array for 40 ms during each spacecraft rotation. The linear, 256-element detector array is aligned north–south (parallel to the satellite's axis of rotation), and the mirror-pointing direction is moved by one pixel in the east–west direction after every spacecraft rotation, building up a complete scan of the Earth in 256 × 282 pixels. This takes approximately 3 min.

The blackened detector array is sensitive to radiation at all wavelengths, though only wavelengths longer than about 0.32 μm carry significant energy in the reflected sunlight, due to absorption by the ozone. Alternate scans observe either the total spectrum of radiation from the Earth (TOTAL channel) or are measured through a quartz shortwave (SW) filter, which transmits only wavelengths that are shorter than 4.0 μm (SW channel). The longwave (LW) measurement is obtained by the subtraction of adjacent TOTAL and SW measurements during ground processing.

The output from the detector array is sampled for 40 ms three times during every spacecraft rotation: when the input beam is coming from the Earth

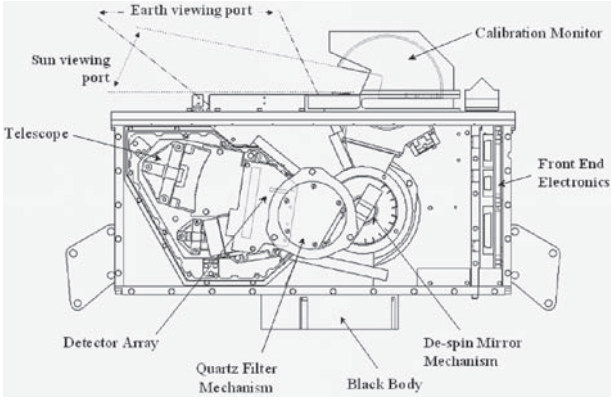

Fig. 2. Layout of the GERB optics unit, as seen from above. Input from the Earth-viewing port, calibration monitor, and blackbody is directed toward the detector array via the despin mirror and telescope optics. Rotating the quartz filter into the path of the beam prevents LW radiation (with wavelength > 4 μm) from reaching the detector.

Table 1. Suppliers and manufacturers of instrument components

Component	Supplier
Optics unit	RAL, UK
Electronics unit	RAL, UK
Detector	Honeywell, Inc, UK
Blackbody	AEA Technologies, UK
Calibration Monitor	RAL, UK
Telescope	AMOS, Belgium
Despin mirror and quartz filter mechanisms	Alenia Difesa - Officine Galileo, Italy
Detector focal plane assembly	Leicester University, UK

Table 2. GERB design specifications.

Wave bands	TOTAL	0.32 μm–>100.0 μm	
	SW	0.32 μm–4.0 μm	
	LW (by subtraction)	4.0 μm–>100.0 μm	
Radiometry		SW	LW
	Absolute accuracy	<1.0%	<1.0%
	Signal/noise	1250	400
	Dynamic range	0–380 W m^{-2} sr^{-1}	0–90 W m^{-2} sr^{-1}
Spatial sampling	44.6 km (north–south) × 39.3 km (east–west) at nadir		
Temporal sampling	15-min SW and LW fluxes		
Cycle time	Full Earth disc, both channels in 6 min		
Coregistration	Spatial: 3-km w.r.t. SEVIRI at satellite subpoint Temporal: within 15 min of SEVIRI at each pixel		
Instrument mass	25 kg		
Power	35 W		
Dimensions	0.45 m × 0.2 m × 0.2 m		

view, the SW calibration monitor, and the BB. Pairs of adjacent TOTAL and SW Earth-viewing scans are calibrated and converted to radiance using the BB scans and views of space obtained before and after each scan of the Earth. The level 0 scans, consisting of calibrated radiance in the TOTAL and SW channels are geolocated, rectified, converted to fluxes, and then binned or averaged in ground processing. Because the same telescope and detector are used to make measurements in the two spectral bands, pairs of scans can be precisely spatially coregistered, but may be separated in time by up to 6 min.

GROUND SEGMENT SYSTEMS AND DATA PROCESSING. *Data processing, access, and archive systems.* The GERB ground segment is distributed between several institutions, as illustrated in Fig. 3. EUMETSAT provides the primary ground station for *Meteosat-8*, handling all communications, including the transmission of commands to the GERB instrument and reception of GERB raw data. The RAL GERB Ground Segment Processing System (GGSPS) receives raw GERB data packets from the primary ground station approximately every 0.6 s and buffers these packets into level 0 (raw telemetry data) product files spanning one TOTAL or SW scan. These level 0 files are calibrated and geolocated to produce level 1.5 (filtered TOTAL and SW radiances) data in NRT, which are then forwarded to the Royal Meteorological Institute of Belgium (RMIB) in Brussels, Belgium. At RMIB the level 1.5 radiance products are converted to level 2 SW and LW radiances and fluxes, incorporating additional information from SEVIRI. The main elements of the processing are shown in Fig. 4 and are described in more detail below. The data products are summarized in Table 3.

The GGSPS product archive consists of a 2.3-terabyte disk storage system, in which the entire current version of the dataset is available online at all times. A searchable catalogue of data products is continually updated, and users may search and download data products via the GGSPS Web site (online at http://ggsps.rl.ac.uk) as soon as they become available. Level 1.5 products are typically available approximately 35 min after the first packet of the file is transmitted from the instrument. Level 2 flux products are generated by the RMIB and are available from there for 40 days after their generation, when they are sent to the GGSPS for access and long-term archive. Potential users are encouraged to register at the GGSPS Web site for timely notification of the official data release in 2005.

Reprocessing exercises will be undertaken in response to the availability of improved calibration data or algorithms for calibration, improved geolocation, or other aspects of science processing, and, of course, are subject to funding. Versions of data and all information pertaining to processing changes will be available from the GGSPS Web site.

Level 1.5 radiance processing. CONVERSION OF RAW DATA TO CALIBRATED RADIANCES. The output from the digital signal processing system from each detector element is used to estimate the steady-state voltage output from each element, accounting for the relevant detector time constant. This is done for the BB, Earth, and calibration monitor (CM) views. The Earth view readings are then converted into filtered radiances, using gains and offsets that are computed from data from the BB and views of space.

These are currently updated for each pair of scans, at approximately 6-min intervals. Analysis of the instru-

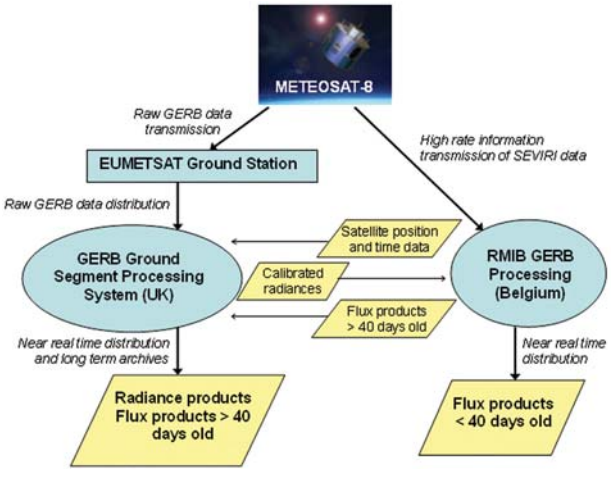

FIG. 3. Near-real-time data flow between the satellite platform, ground station, and processing systems at the Rutherford Appleton Laboratory and the Royal Meteorological Institute of Belgium.

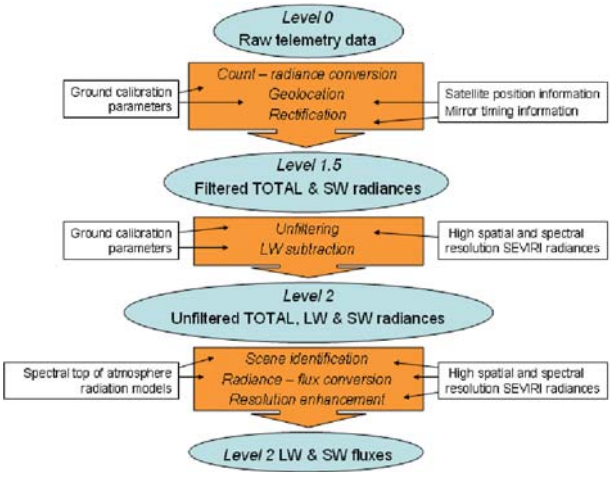

FIG. 4. Summary of data processing from level 0 telemetry data to level 2 fluxes, showing processing steps and auxiliary data required at each step.

ment performance to date shows that these calibration parameters do not show significant variation with time, as seen in the instrument in-flight evaluation. This update frequency may, therefore, be reduced in future processing versions to prevent spurious variation from being introduced by the in-flight features discussed below.

Geolocation and rectification. Each view of the Earth is geolocated, meaning that a latitude and longitude is determined for the point where the line of sight of each pixel intersects the surface of the Earth. This requires knowledge of the satellite position and timing information to determine GERB's pointing direction. The satellite position and orientation is determined to high accuracy by SEVIRI processing using landmark and horizon information. The SEVIRI header files containing this information are routed via the RMIB ground segment. Timing information in the GERB data is used to determine the phase of the despin mirror and, hence, the east–west position of the GERB detector column relative to the Earth. The relative pointing directions of the 256 GERB detector elements have been determined from preflight calibration point spread function (PSF) measurements, with corrections for post-launch misalignments.

Table 3. Primary scientific data products available from the GERB GGSPS at RAL and the RMIB Online Short-term Services (ROLSS). All products are in Hierarchical Data Format and include geolocation information. Data products at Level 2 BARG and above are corrected for the instrument PSF, giving "exact" 50-km resolution.

Product name	Description	Content	File size	Spatial resolution	Averaging and binning times	Processing system	Archiving system
Level 1.5 NANRG	Nonaveraged, nonrectified, and geolocated	Filtered SW and TOTAL radiances	2.9 MB	Nominal 50-km resolution at nadir	"Instantaneous" radiances—six scans per file	GGSPS	GGSPS
Level 1.5 ARG	Three-scan average, rectified, and geolocated	Filtered SW and TOTAL radiances	1.3 MB	Nominal 50-km resolution at nadir	Approx 17-min average based on six nonaveraged, nonrectified geolocated (NANRG) scans	GGSPS	GGSPS
Level 2 ARG	Three-scan average, rectified, and geolocated	Solar and thermal unfiltered radiances and fluxes, scene identification	1.3 MB	Nominal 50-km resolution at nadir	Approx 17-min average based on six scans	RMIB GERB processing (RGP)	RMIB On Line Short Term Services (ROLSS) within 40 days of creation; GGSPS thereafter
Level 2 BARG	15-min bins, averaged, rectified, and geolocated	Solar and thermal unfiltered radiances and fluxes, scene identification	1.6 MB	Exact 50-km resolution at nadir	Exact 15-min bins in average	RGP	ROLSS within 40 days of creation; GGSPS thereafter
Level 2 SHI	Snapshot high-resolution image	Solar and thermal unfiltered radiances and fluxes, scene identification	37 MB	3 × 3 SEVIRI pixel resolution	15-min snapshot, at SEVIRI times	RGP	ROLSS within 40 days of creation; no long-term archive
Level 2 monthly means	Monthly average, rectified, and geolocated	Solar and thermal clear- and all-sky fluxes		Exact 50-km resolution at nadir	Averages over one calendar month	GGSPS	GGSPS
Level 2 binned monthly means	15-min-binned monthly average, rectified, and geolocated	Solar and thermal clear- and all-sky fluxes		Exact 50-km resolution at nadir	Exact 15-min bins over one calendar month in average	GGSPS	GGSPS

Deviations of the satellite platform from an ideal geostationary orbit, and a small nonrepeatability in the motion of the scan mirror, mean that the points measured by successive scans are in slightly different positions on the Earth's surface. In order to average different scans together, the data are first rectified, that is, interpolated onto an equiangular geocentric grid as viewed from the ideal satellite position and orientation. The instrument spatial sampling resolution gives a subsatellite pixel of 44.6 km (north–south) × 39.9 km (east–west), which becomes 50 km × 50 km in the rectified grid. Instrument PSF is not corrected for in level 1 rectification. Target geolocation accuracy is 0.1 pixel, and the actual accuracy is being established in validation activities.

Level 2 radiance and flux processing. RADIANCE UNFILTERING. Variations of the instrument sensitivity with wavelength are removed in the unfiltering process. Accurate estimation of the unfiltered reflected solar and emitted thermal radiances from the filtered radiances requires information about the spectral signature of the incoming radiation. This information is provided by the SEVIRI imager's narrowband measurements. The unfiltered and filtered radiances L^{uf}_{SEV} and L^{f}_{SEV}, respectively, are estimated from the imager through narrowband-to-broadband conversions and convolution with the GERB PSF and spectral response. The unfiltered radiances L^{uf} are then calculated from the filtered GERB measurements L^{f}_{GERB} using

$$L^{uf} = L^{uf}_{SEV}\left(\frac{L^{f}_{GERB}}{L^{f}_{SEV}}\right). \quad (1)$$

Using a database of TOA spectral radiance curves (Clerbaux et al. 2003), the 1-σ error introduced by the unfiltering process has been determined to be about ±0.3% for solar and ±0.1% for thermal radiation.

SCENE IDENTIFICATION AND CLOUD MASKING. To convert radiance (L) into flux (F), the scene in each pixel is characterized in terms of surface-type and cloud cover properties, retrieved from SEVIRI. This takes advantage of accurate clear-sky reflectance in the 0.6- and 0.8-μm visible SEVIRI channels (Ipe et al. 2003). For each SEVIRI pixel, the cloud optical depth (τ) is retrieved from the reflectance using lookup tables, described in Ipe et al. (2004). Using the Streamer radiative transfer model (Key and Schweiger 1998), 24 lookup tables have been built—for the two SEVIRI visible channels, ice and water clouds, and for six surface types. The cloud phase is retrieved from the 12.0-μm brightness temperature and from the 1.6-μm reflectance using a method similar to Nakajima and King (1990). A cloud mask is derived at the SEVIRI pixel resolution by thresholding the cloud optical depth, and the cloud fraction over the GERB footprint is then estimated from this mask. The threshold ($\tau = 0.9$) was chosen for consistency with the CERES cloud fraction retrieval (Ipe et al. 2004).

RADIANCE-TO-FLUX CONVERSION. The flux is estimated from the unfiltered radiance using models of the angular distribution of the radiant energy at the TOA. Models from the CERES instrument on board the Tropical Rainfall Measuring Mission satellite (Loeb et al. 2003) are used in the SW, while for the LW a method based on the SEVIRI thermal channels has been developed (Clerbaux et al. 2003). Like the unfiltered radiance, the fluxes are first estimated from SEVIRI (FSEV), then convolved to the GERB footprint, and finally corrected using the radiance-unfiltering correction factor L^{f}_{GERB}/L^{f}_{SEV}.

RESOLUTION ENHANCEMENT. During resolution enhancement, the quantities L^{f}, L^{uf} and F are transformed from the GERB resolution, nominally 50 km at nadir, to a 3 × 3 SEVIRI pixel resolution, nominally 9 km at nadir (Gonzalez et al. 2000). Resolution-enhanced unfiltered radiances and fluxes are produced every 15 min.

Monthly means. Monthly mean products are of value in allowing direct comparison with the monthly mean data from polar-orbiting instruments. These will be generated from level 2 all-sky and clear-sky fluxes. Two products are planned: first, the monthly mean itself; and second, a mean of 15-min bins from each day, that is, a monthly mean of the diurnal cycle. Monthly mean products are not yet available, though once routine processing capability has been established, average products will be generated from the start of the science data record.

INSTRUMENT CALIBRATION.

Preflight calibration. Knowledge of the GERB TOTAL and SW channel spectral response (the product of instrument throughput and detector responsivity) is required for converting the measured detector voltages into radiances for the TOTAL, SW, and LW channels (Mossavati et al. 1998). The measurements necessary to formulate this spectral response were made during the preflight ground calibration undertaken in the Earth Observation Characterisa-

tion Facility at Imperial College. The BB used for in-flight calibration was characterized as a function of temperature and was linked via a transfer standard to the national absolute standard. Also, the PSF, a measure of the angular response, was measured for each individual detector element. These measurements were made consistent with the target in-flight measurement accuracies of ±1% in SW and LW radiances (see Table 2).

The spectral responses of the TOTAL and SW channels were determined by combining spectral measurements of each individual component of the optical system: mirror reflectance, quartz filter transmission, and detector responsivity. The mirror and filter data were combined to produce a telescope optical model giving the transmittance per channel per detector element. These transmittances were multiplied by the detector data to produce a final spectral response for each channel and each detector element. The telescope measurements were made over the wavelength range of 0.3–140 μm. The detector measurements were made using band pass filters to isolate different narrow spectral ranges over the range of 0.3–25 μm, and were combined with measurements from 2.5 to 55 μm of the reflectivity of witness samples (metal substrates with similar black coatings). These were then extrapolated to produce a detector response from 0.3 to 140 μm. Further details of the instrument calibration will form the basis of a subsequent publication.

The calibration algorithms assume a linear relationship between detector output and filtered radiance. This assumption was tested for a subset of detector elements using a visible light source and a narrowband filter over the full instrument dynamic range in both channels. Additionally, all detector elements were checked in the TOTAL channel using a variable temperature BB for a subset of the instrument dynamic range. Figure 5 demonstrates the highly linear nature of the instrument response, showing the correlation coefficient between the incoming radiance and response per detector element of between 0.99997 and 1.00000 (except for one element at 0.999965). The spectral characterization used three calibration sources, supplied by the U.K. National Physical Laboratory, with calibrations traceable to national absolute standards. Two BB sources were used: one at about 300 K, representing an Earth-like source, and the other at liquid nitrogen temperatures, approximating an in-flight deep-space view. The third source was a lamp-illuminated integrating sphere, with an effective temperature of 310 K representing the visible and near-IR solar spectrum region.

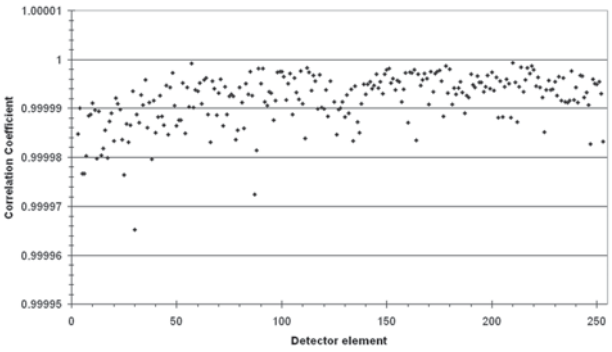

Fig. 5. Correlation coefficient between LW input signal and instrument response, as measured during preflight calibration, showing a high degree of linearity.

The internal BB was also calibrated for all detector elements using the two BB sources over the range of predicted in-flight temperatures.

The SW channel point spread function for each detector element was measured using a highly collimated incident beam from a HeNe laser (wavelength 633 nm) to produce a focussed spot at the detector. The spot was stepped in small increments in two orthogonal axes in the detector plane to obtain a grid of width ±3 pixels around each detector element. These data were adjusted for predicted optical distortions due to the satellite spin rate, and were combined with the system optical model to derive a LW channel PSF for each detector element.

In-flight calibration updates. The instrument is continually calibrated in flight using BB and space views, as described in the data processing section. This provides an accurate, absolute calibration of the thermal response of the instrument throughout the infrared. Maintaining the required measurement accuracy in the SW spectral range is, however, more of a problem, which is well known in ERB experiments. This problem arises primarily because of the impracticality of using a calibration target that is close in brightness temperature to that of the sun. However, an integrating sphere, illuminated at certain geometries by the sun, can be used as a monitor of spectral response changes in the SW channel. Such changes can arise from degradation of the quartz filter or the mirrors, as well as the detector response.

The onboard CM consists of an integrating sphere, whose output aperture is scanned once every satellite rotation, after the Earth view. A specific scan mode is also run 4–6 times a year under optimal illumination conditions. This mode is used to determine changes in the filter response over the lifetime of the mission and as input to update calibration parameters.

The spectral reflection properties of the CM may also change throughout the course of the mission due to degradation of the aluminium surface, primarily in the UV. Changes in this response are monitored using three photodiodes that are mounted close to the output aperture, measuring continuously in the UV, visible, and near-infrared. Combining the daily CM-illuminated scan data with photodiode spectral information will allow characterization of any spectral changes occurring within the CM itself. Results after a year of operation show that the CM is spectrally stable to date.

Checks of the ground measurements of detector PSF are made in flight, because postlaunch distortion of the optics and satellite spin axis changes due to spacecraft maneuvers may affect the PSF. The instrument linearity is also checked at regular intervals in flight, by changing the BB temperature while scanning deep space.

INSTRUMENT IN-FLIGHT PERFORMANCE. GERB has been operating and under validation for 2 years and has been performing very successfully. Figure 6 shows the "first light" filtered radiance images from GERB, collected on 12 December 2002. The high quality of the images, and the correct performance of the scanning and calibration procedures were immediately evident from these early data.

Mirror-pointing accuracy. In order to meet the scientific goals of GERB the mirror-pointing position should be known to 0.8 arcmin. The position of each successive scan line is measured by GERB with respect to a signal provided by the spacecraft platform, which is used to derive information on the position of the Earth relative to the spacecraft, known as the start of line pulse (SOL), for every rotation. There are two main components to instrument-pointing accuracy: the error in the GERB mirror position measurement, and the error in the spacecraft SOL signal. The mirror measurement has been verified to have a repeatability of better than 0.4 arcmin (0.1 step size or pixel width). Currently, however, the SOL pulse has systematic errors of up to 6 arcmin (1.5 steps). A temporary solution has been implemented in the GGSPS processing, and considerable effort is being expended to understand and correct for these errors so that they can be reduced even further to meet the overall pointing requirement.

Both sides of the mirror are used to acquire data. During instrument-commissioning activities, an angular offset of 0.3 arcmin between the two mirror faces was detected. This has been corrected for in onboard software, and the effect on the measurement is now negligible.

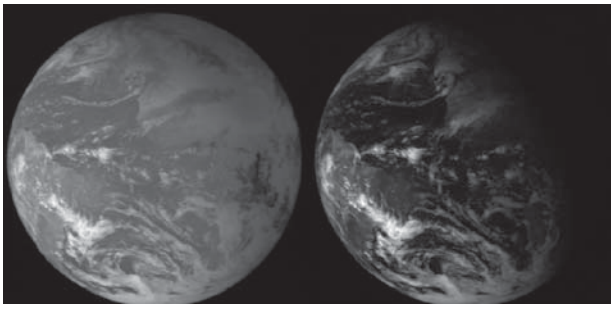

Fig. 6. GERB first light images from 12 Dec 2002 in (left) TOTAL and (right) SW channels. Cloud and weather systems and the underlying land and ocean surfaces are clearly visible in the illuminated part of the SW image. Western North Africa is visible under the terminator and eastern South America at the left-hand side of the disc. The features visible in the illuminated part of the TOTAL channel image are very similar to the SW channel, but with less contrast due to the addition of the LW signal. The signal in the nighttime part of the TOTAL channel is due to broadband LW radiation, and is dominated by the thermal emission from atmospheric water vapor.

Stability of instrument in flight. Analysis of calibration data collected to date has shown that both the SW and the LW responses of the instrument have been stable in the initial year of operation. These parameters are continually monitored, and any drift in sensor response can be characterized and accounted for in the processing. The thermal environment of the instrument is within the predicted range of temperatures and shows only very small variations from day to day outside the equinox season. During equinoxes, and for a period of 3–4 weeks before and after, the instrument cools rapidly when the sun is eclipsed by the Earth at midnight. External temperatures can change by up to 15°C over 2 h. Temperatures inside the instrument are controlled by heaters, however, with a maximum variation of 1°C in the same time frame. Power supply from the satellite platform and distribution within the instrument has also been very stable and within specification to date.

Detector noise. A deep space-scanning mode considerably extends the amount of space data that are acquired during each scan. These data allow for the evaluation of the stability of the instrument gain under conditions of varying BB temperature and determination of the instrument noise level. Although the gain is calculated every 5 min, so that gain stability over a 12-h period is not a requirement

for accurate calibration, in fact, the gain is stable over this time. For all detector elements, the distributions of gain with time are narrow and sharply peaked with standard deviations around 0.3%. This indicates that instrument noise is very low, and within budget.

Stray-light features. The above-mentioned eclipse of the sun at equinoxes has unavoidable consequences for GERB operation. Direct illumination of the detectors would cause permanent damage, and the instrument must be safeguarded from such events. Because the instrument pointing can only be controlled in the east–west direction, data collection must be shut down during periods when the solar declination brings it within the field of view (FOV) in order to ensure instrument safety. This results in loss of data for 4–5 h every night, centered around local midnight for 5–6 weeks before and after spring and autumn equinoxes. For 2 weeks before and after these periods, the data around midnight are affected by reflection of stray solar illumination within the instrument cavity as the sun approaches the FOV. This stray light is a significant fraction of the radiance that is measured for 2 h, again centred around local midnight.

Internal reflection of solar illumination has also been shown to affect the BB radiances, for approximately 1.5 h around 1130 UTC every day. The BB radiances are currently used continuously for calibration of the measured Earth radiances, so this, in turn, affects the accuracy of the data products. Solutions to both of these stray-light problems are currently being investigated, and the data that are affected will be flagged.

VALIDATION AND SCIENCE PLANS. *Validation plan.* Validation of as many of the GERB data processing steps and intermediate products as possible is planned, as well as evaluation of the final unfiltered radiance and flux products by intercomparison with other observations and models, internal consistency checks, and the use of ground measurements.

Special instrument-scanning modes have been designed to monitor pixel noise and SW sensitivity; validate ground calibration measurements of PSF and time response; and evaluate the accuracy of particular processing steps, for example, interpolation and averaging.

The radiance mode of the Met Office Unified Model, which simulates the measurements made by different instruments, will be used to provide a transfer standard between GERB detectors and other sensors. Time series comparisons between model and GERB fluxes over well-understood scenes, for example, a clear ocean, can also be used to highlight changes in the instrument performance (Allan et al. 2004).

Measurements of broadband LW and SW radiances and fluxes made by the CERES instruments can also be employed for validation. Special programmable scanning modes enable CERES to vary its scanning pattern to increase the number of observations that match the GERB viewing geometry (Smith et al. 2003). This is particularly important for the comparison of the highly anisotropic SW radiances. GERB and CERES unfiltered radiances and scene identification can be compared for collocated and coangular observations. Additionally, fluxes can be compared for collocated observations for different viewing angles, as a function of observation angle. Such comparisons can provide a transfer standard between GERB detectors; more detailed comparisons, at well-characterized sites and involving other instruments, can provide a simultaneous and independent measure of the accuracy of both instruments.

The validity of the theoretical basis and algorithms that are used for radiance unfiltering and radiance-to-flux conversion (described in the section subtitled "Level 2 radiance and flux processing") can also be confirmed by directly applying these algorithms to the broadband-filtered radiances, measured by CERES, and comparing the results with the previously validated CERES products.

While broadband measurements from CERES provide the most direct comparison, narrowband measurements, made by other satellites, can also be used for validation. Through modelling, broadband radiances and fluxes can be derived from narrowband radiance measurements. Comparing these to CERES-measured radiances, as well as GERB measurements, allows for the separation of differences due to GERB calibration from those due to spectral modelling. Repetition of the comparison for GERB products at different spatial resolutions, and for varying temporal interpolation, allows the errors in resolution enhancement and temporal interpolation to be investigated. Additionally, day–night variability in the comparisons can be used to evaluate the accuracy of the TOTAL–SW subtraction, used in calculation of the daytime longwave products.

Well-characterized sites will be used for long-term monitoring and for intercomparisons with different instruments and models. In the SW, stable desert sites will be used. In the LW, high clouds can be used because they lie above much of the atmosphere and their signal is close to that of a blackbody, which simplifies the modelling required. Comparisons will also be made for clear-sky ocean scenes, particularly where

nearby atmospheric profiles and surface temperature estimates are available. Large-scale calibration sites, such as those in the Valencia and Castilla-La Mancha regions in Spain, will be used in conjunction with ground measurements for detailed intercomparison exercises. Participation in field campaigns measuring atmospheric radiation and state will also be part of the validation process.

Initial results. The validation process is ongoing, and here we report the preliminary results of intercomparisons between the GERB and CERES unfiltered reflected solar and emitted thermal radiances that are matched for time, space, and viewing geometry. Comparisons have been made over all detectors that are separated by SW scene type, and individually for each of the 256 GERB detectors.

The comparison for all GERB detectors found a GERB/CERES LW radiance ratio of 0.997 ±0.007 (all results quoted at a 95% confidence interval). The reflected SW data were separated according to five scene types, with distinct spectral radiance distributions and brightness levels. The best correspondence was found for clear-sky bright deserts, for which the GERB/CERES ratio was 1.001 ±0.010 and the clear-sky ocean was the worst case with a ratio of 0.931 ±0.009. The instrument spectral characterization is the most likely cause of these scene-dependent differences and these data are currently being reanalyzed.

To further investigate the SW radiance discrepancies a comparison was made by separating by GERB detector rather than scene type. The GERB detector array is oriented roughly north-south with respect to the Earth; each GERB pixel, therefore, views a large range of longitudes but only a small range of latitudes. Figure 7 shows the detector-based SW results for data obtained around the Northern Hemisphere winter solstice 2003 (black) and the 2004 summer solstice (red). Figure 7a shows the number of matched points used; Fig. 7b shows the average SW radiances observed for each of the GERB detectors (solid lines) and the corresponding matched CERES points (dashed lines) and Fig. 7c shows the average GERB/CERES ratio. This comparison did not discriminate between scene types, which introduce much of the variability in the results. It should also be noted that the difference in spatial resolution of the two sensors is most marked at higher latitudes, corresponding to the outermost GERB detectors. Below detector number 20 and above detector number 230 the number of matched points decreases, affecting the robustness of the comparison.

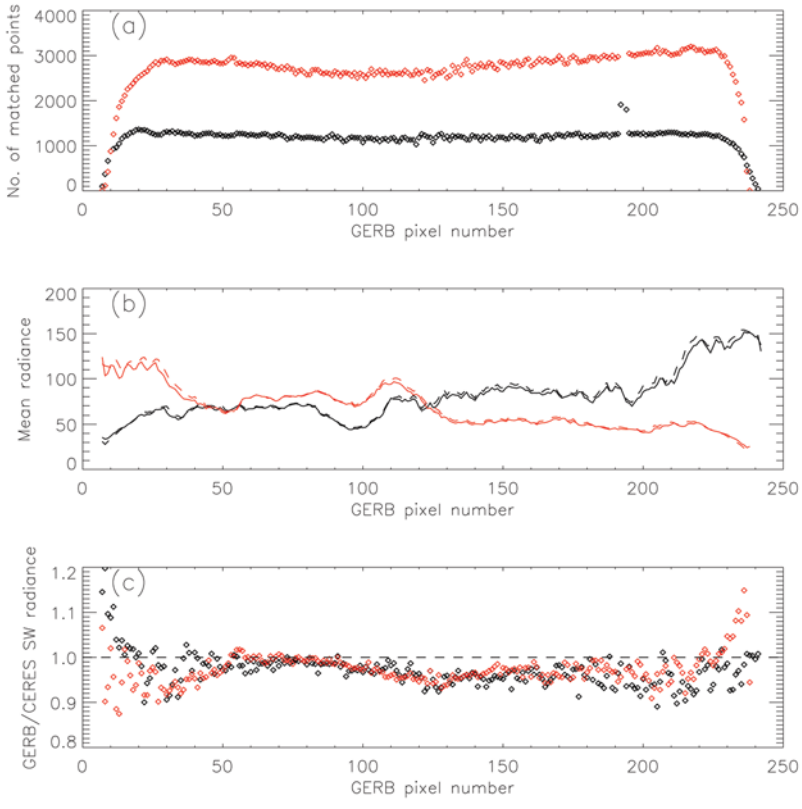

Fig. 7. Results of SW radiance comparison for GERB and CERES data collocated in time and space and matched for viewing geometry obtained during Northern Hemisphere 2003 winter solstice (black) and 2004 summer solstice (red) intercomparison campaigns. (a) The number of points matched for each of the GERB detectors, (b) the average GERB (solid line) and CERES (dashed line) observed for each of the GERB pixels, and (c) the mean GERB/CERES SW radiance ratio for each of the GERB detectors are shown.

In general, the results indicate that GERB measures a lower SW radiance than CERES. For GERB detectors from 50 to 200 the difference is generally 5 W $m^{-2}sr^{-1}$ or less, however, the GERB/CERES ratio shows a clear variation over the detector array that appears quite repeatable from summer to winter for these central detectors. Some of this variation reflects differences in the geographical regions observed; for example, the good agreement for detectors 70–80 may be due to the fact that these detectors pass over

the Sahara, which consists primarily of the scene type that gave the best agreement in the previous comparison. It is also possible that some of the structure is due to artifacts introduced by the GERB instrument, this is being investigated further.

SCIENCE APPLICATIONS. *Cloud radiative forcing.* Clouds, cloud processes, and the feedbacks associated with them, represent one of the primary sources of uncertainty in predicting our future climate. One approach to improve this situation is the accurate quantification of the effects of cloud in the current climate. Cloud radiative forcing, calculated as the difference in the energy balance between clear-sky and cloudy conditions, is a commonly used tool. Results from ERBE enabled estimation of the global mean cooling effect of clouds to be around 15 W m^{-2} (Ramanathan et al. 1989), with substantial regional variations related to differences in cloud type and large-scale dynamics. The use of traditional monthly mean cloud forcing data to study a particular cloud or dynamical regime, such as tropical convection, is limited by averaging over all weather systems and cloud types occurring during a month, however. In a comparison of the Pacific warm pool and African/Atlantic tropical regions (Futyan et al. 2004), differences in monthly mean behavior could not be attributed to differences in convective cloud properties, because low nonconvective cloud was present on some days during the month in parts of the African "convective" region.

Combining high-resolution ERB data from GERB with cloud classifications based on coregistered SEVIRI data provides information on the radiative impacts of cloud systems at time scales that are comparable to those on which they develop. By averaging only observations for a particular cloud type or other condition, the behavior associated with different regimes occurring during a month can be separated (Futyan et al. 2005). This approach will enable differences between regions to be more fully understood and provides valuable additional information for the validation of climate and NWP models.

Aerosol radiative forcing. Quantifying both the direct and indirect impact of aerosols is one of the major challenges facing climate scientists today. Uncertainties in concentrations and the radiative and chemical properties of the various aerosol types hinder estimates of both effects. In addition, their relatively short lifetimes and complex geographical distributions put stringent requirements on the sampling rate and coverage required to monitor their presence effectively.

The combination of GERB and SEVIRI on *Meteosat-8* provides a powerful tool for detecting aerosols and estimating their radiative effect at high temporal and spatial resolution. Although climatologies of aerosol properties do exist for the area viewed by the satellite, these are based on data from polar-orbiting platforms and, hence, suffer from poor diurnal sampling. GERB and SEVIRI data will provide the first opportunity to measure the effect that short-term aerosol variability has on the Earth's radiation budget over the *Meteosat-8* field of view. The rapidity of observations should also permit investigations into the impact of aerosol on cloud development and radiative properties.

According to the 2001 Intergovernmental Panel on Climate Change report (Houghton et al. 2001), the largest uncertainties in aerosol direct radiative forcing are associated with mineral dust. On a global scale, the Sahara is the most important source of desert dust (Washington et al. 2003). A methodology for detecting dust aerosol using SEVIRI LW channels is

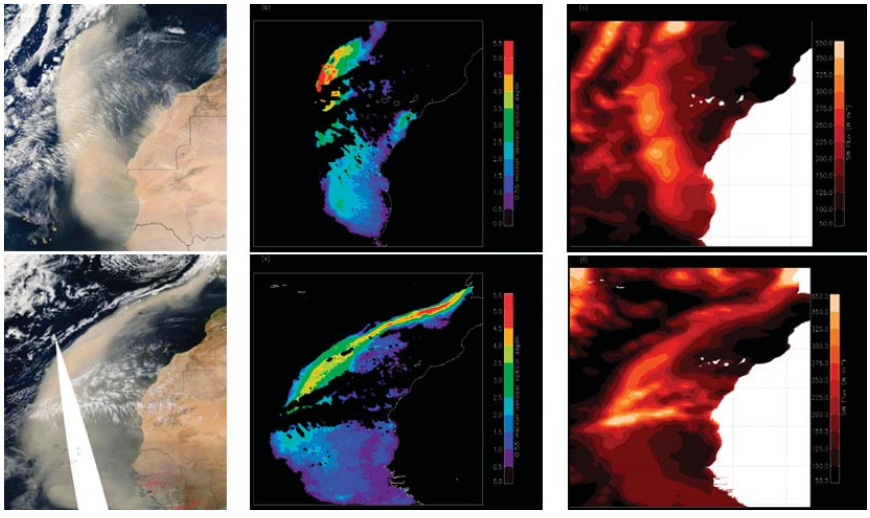

Fig. 8. Saharan dust outbreak over the Atlantic Ocean as seen at (top) 1155 UTC, 4 Mar 2004 and (bottom) 1405 UTC 5 Mar 2004. (a), (d) The true color MODIS images from the *Terra* and *Aqua* satellites, respectively; (b), (e) the retrieved 0.55-μm aerosol optical depth from SEVIRI for the nearest available time slot; (c), (f) the corresponding GERB-reflected TOA shortwave flux.

being developed at Imperial College (Brindley 2004). Figure 8 shows results obtained for a dust outbreak over the Atlantic seen earlier this year. Two time slots are shown—1200 UTC 4 March (upper), and 1400 UTC 5 March (lower). The left-hand panel in each case shows a true color image obtained from the Moderate Resolution Imaging Spectrometer (MODIS) within 5 min of each observation, while the middle panel indicates the retrieved SEVIRI 0.55-μm optical depth. The right-hand panel shows the corresponding reflected solar flux as measured by GERB. Some caution should be attached to the absolute values of the GERB fluxes, because at present the radiance-to-flux conversions used in the GERB processing do not explicitly account for aerosol. Nevertheless the signature of the dust plume is apparent in the observations, and the potential for improving radiative forcing estimates is clear. A separate algorithm using the visible and near-infrared SEVIRI channels is currently under development and will be employed both as a check on the LW methodology for dust detection, and, in concert with the GERB observations, to evaluate the impact of other aerosol types (such as those produced as a result of biomass burning) on the radiation budget.

Diurnal effects. A major source of uncertainty in the estimation of even monthly averaged ERB quantities is the limited temporal sampling that is possible from low Earth-orbiting satellites. Even under clear-sky conditions, models have to account for the diurnal variations of albedo and outgoing LW radiation (OLR) that are associated with changing solar zenith angle and surface temperatures through the day. In cloudy conditions, accounting for the often coherent diurnal variations in meteorology is even more challenging. For existing ERB datasets, a range of assumptions have been made (Young et al. 1998), introducing uncertainty in the mean flux estimates. GERB's unique ability to fully resolve these diurnal variations removes the need for such assumptions, at least in the all-sky case.

GERB monthly averaged flux products (planned for future release) will, therefore, be the most accurate and least model-dependant diurnally averaged fluxes available. A monthly mean diurnal cycle product will also provide unique information on the coherent diurnal variations found across the GERB field of view. This information provides a valuable validation, and potential means of improvement, of the models currently in use. Development of clear-sky interpolation algorithms indicates the possibility of improvements to the half-sine model used for interpolation of clear-sky LW fluxes over land in ERBE and CERES processing (Futyan and Russell 2005).

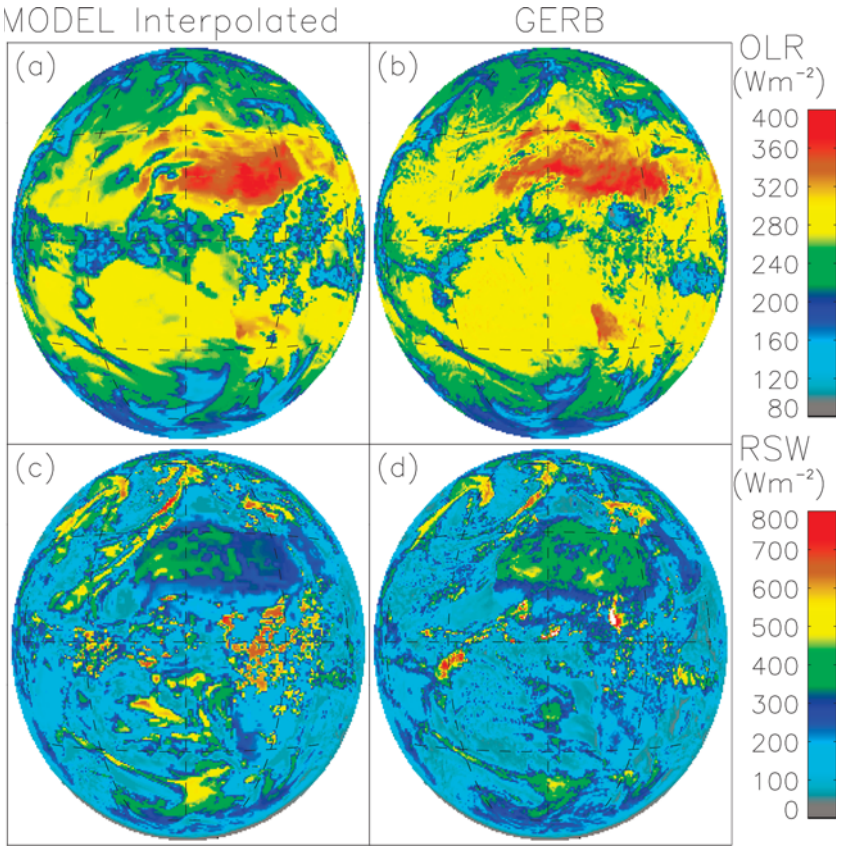

Fig. 9. Outgoing longwave radiation (upper) and shortwave reflected radiation (lower) for the UK Met Office numerical weather prediction model (left) and GERB (right) for 1200 UTC, 21 Apr 2004.

Comparison with numerical models and other sensors. A very important application for GERB data is the provision of accurate, independent, high-temporal-resolution data for the evaluation of numerical models. The first results are from the Simulations from a NWP Model to Exploit Radiation Data from a New Geostationary Satellite, Explore Radiative Processes, and Evaluate Models (SINERGEE) project (Allan et al. 2004). Diagnostics

from the Met Office operational numerical weather prediction model (Bell et al. 2002) are transmitted regularly to the Environmental Systems Science Centre, allowing comparisons with the corresponding GERB data within about a day of the observation time. Initial results use operational analyses for 0000, 0600, 1200, and 1800 UTC. Figure 9 shows an example of comparisons between the broadband OLR and reflected SW radiation (RSW) from GERB and the model for 21 April 2004. In this example, the model data are interpolated onto the GERB grid.

The model shows good agreement with the data at high latitudes, which indicates two important points. First, the large-scale dynamical structure is well represented, leading to realistic humidity distributions. Second, the model cloud parameterization scheme converts this information into realistic cloud fields (see also Ringer et al. 2003). At low latitudes, however, the link between the large-scale dynamics and clouds is weaker, and there are fewer observations to constrain the model, which shows much larger errors in the cloud fields. Note, for example, the excessive deep convective cloud over Africa at this time of day, consistent with known errors in the modelled diurnal cycle of convection (Yang and Slingo 2001; Slingo et al. 2004). The RSW comparisons reveal excessive amounts of subtropical marine stratocumulus. Over the Sahara, the modelled RSW is too low, suggesting errors in the surface radiative properties. These results illustrate the potential of such analyses for revealing systematic errors in the model. It is planned to extend this analysis to include model forecasts and comparisons with radiances from the SEVIRI imager.

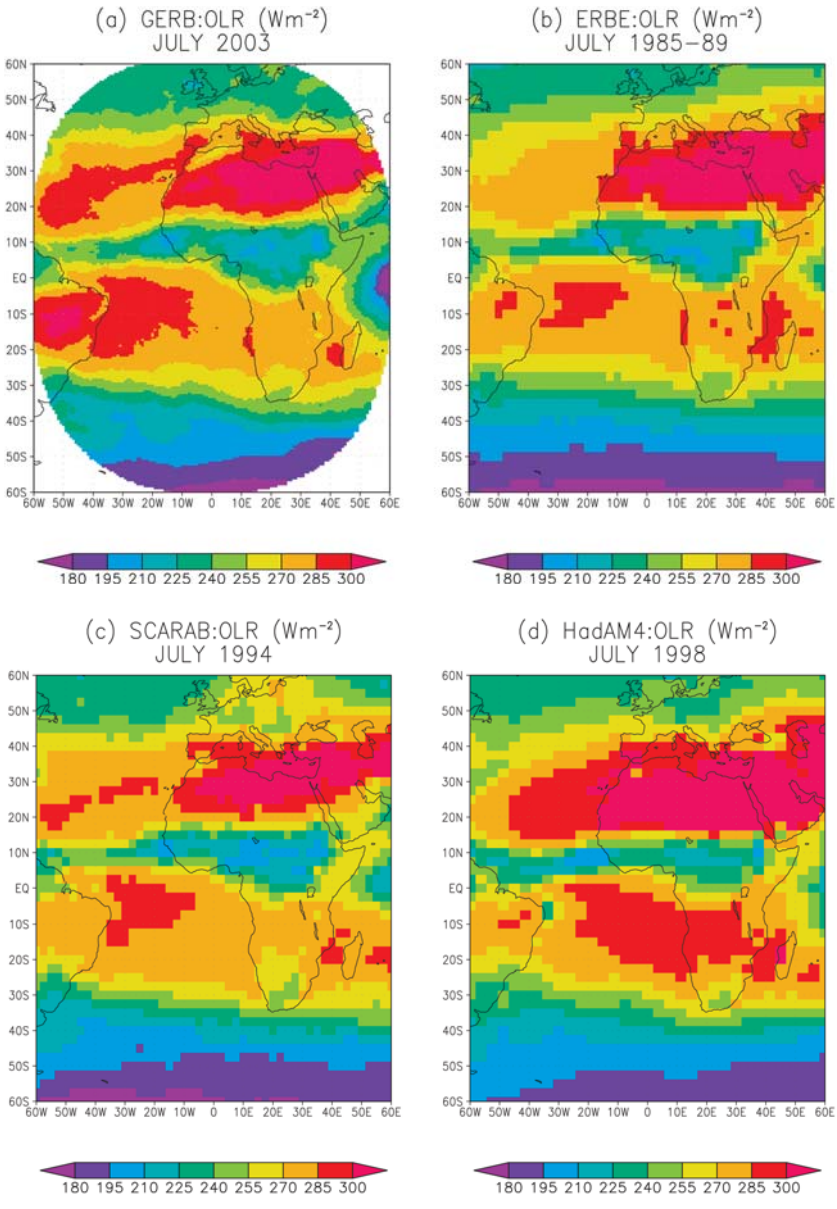

Fig. 10. Monthly mean OLR for Jul (different years) from GERB, the Earth Radiation Budget Experiment, Scanning Radiation Budget sensor and simulations by the Hadley Centre climate model, HadAM4.

Figure 10 shows a comparison of the monthly mean OLR from GERB with earlier data for the July period (though in different years) from the Earth Radiation Budget Experiment (Harrison et al. 1990), with the Scanning Radiation Budget sensor (Kandel et al. 1998), and with simulations by version 4 of the Hadley Centre for Climate Prediction and Research Atmospheric Model (HadAM4) (Pope et al. 2000; Webb et al. 2001). The GERB data do not cover the whole of July 2003 because the instrument was turned off for some of this period; nevertheless, the results compare favorably with the earlier data, and some of the differences may be due to interannual variability. The model reproduces the broad features of the

observations, although some systematic model errors are also apparent, such as the excessive emission in the subtropics, suggesting not enough cloud and/or too dry an atmosphere.

Water vapor feedback. Atmospheric water vapor feedback (WVF) is a matter of some controversy. The majority of studies (but not all) have concluded that this feedback process is positive, increasing the warming that is initially caused by growth in greenhouse gases. For example, Rind et al. (1991) found clear evidence of positive WVF using new satellite-generated water vapor data to investigate this question, concluding that the water vapor feedback is not overestimated in models. More recently, Soden et al. (2002) used the natural experiment offered by the eruption of Mt. Pinatubo to show that the observed thermal and humidity responses to this eruption could not be explained without a strong positive WVF. However, some authors, for example, Lindzen (1990), have argued in a variety of ways that the WVF can, at least in some circumstances, act in a negative sense, to reduce an initial greenhouse gas warming. Recently, Minschwaner and Dessler (2004) used satellite observations and models to suggest that the fixed relative humidity assumption that is usually applied in models is not valid, and that the WVF, though positive, is not as strong as in the models.

Because the OLR is sensitive to water vapor and to temperature, observations of OLR by GERB and SEVIRI, plus measurements of water vapor and temperature from polar orbiters, will be used to study the WVF, by modelling the effect of observed water and temperature profiles on the OLR and comparing these with modelled and observed OLR. The high time resolution of GERB and SEVIRI will allow study of the WVF variability.

CONCLUSIONS. The first GERB instrument has been in operation since December 2002 on board the *Meteosat-8* spacecraft, positioned over 3.5°W and the equator. Further GERB instruments, funded by EUMETSAT, are being developed for the subsequent series of Meteosat Second Generation spacecraft, with the second due for launch in 2005.

Considerable effort went into the unique design and prelaunch calibration of this series of instruments to ensure the high stability and accuracy of the LW and SW flux measurement required for climate and atmospheric processes research. An overview of that design has been given here, and further details on different aspects of the design and development of GERB will be published in subsequent papers.

Validation activities started in December 2002, and the results show the instrument to be performing extremely well. Initial analyses show the instrument performance, in terms of function, calibration, scanning and synchronization with the spinning spacecraft, electronic and data systems, and, most of all, in the quality and accuracy of the data produced, is excellent. The validation process will continue for some time yet, as a deeper understanding of the instrument operation is developed. A dedicated team of scientists and engineers are working to ensure that the best scientific results will be obtained.

The paper has also presented examples of early scientific studies being undertaken by the GERB team. While these studies are being used initially to validate and calibrate these new data, they also demonstrate their potential to establish a wide range of exciting new climate and process science. This is becoming possible with the advent of this new observational tool in our array of instruments with which to study how the Earth's climate system works and how it is developing.

ACKNOWLEDGMENTS. The members of the GERB International Science Team have made considerable contributions to the successful development of this project at all stages, and their activities and continued involvement are greatly appreciated. Many thanks also to the NASA CERES team, whose generosity in sharing their experiences has been most helpful: we value their continuing collaboration.

The U.K. design, development, building, and testing of the first GERB instrument was funded by the Natural Environment Research Council (NERC), with grants to Imperial College, the Rutherford Appleton Laboratory, and Leicester University. NERC also funded the development of the Earth Observation Characterisation Facility, a clean, high-vacuum calibration facility at Imperial College. The team is deeply grateful for the support from NERC and its officials, especially Dr Steven Briggs in its formative stages.

A. Slingo and R. P. Allan's contributions were funded by a joint NERC/Met Office Connect-B grant. M. A. Ringer of the Met Office was funded by the U.K. Department of Environment, Food and Rural Affairs under contract PECD 7/12/37.

The telescope development at AMOS/OIP and part of the Belgian ground segment development at RMIB was funded by the Belgian science policy office through the PRODEX program. Engineers and scientists at Officine Gallileo, Italy, made important contributions, funded by their government. Also, the U.K. National Physical Laboratory provided equipment and expertise for the absolute calibration of GERB.

Finally, the roles of EUMETSAT and ESA in the provision of flight space on board *Meteosat-8*, assisting the GERB project during development, and in postlaunch operations have been crucial. EUMETSAT has provided funding for building and operating *GERB-2*, *-3*, and *-4*. The SEVIRI images are copyright of EUMETSAT.

LIST OF ACRONYMS

BB	Blackbody
CERES	Clouds and the Earth's Radiant Energy System
CM	Calibration monitor
ERB	Earth Radiation Budget
EUMETSAT	European Organisation for Exploitation of Meteorological Satellites
FOV	Field of view
GERB	Geostationary Earth Radiation Budget
GGSPS	GERB Ground Segment Processing System
LW	Longwave
MODIS	Moderate Resolution Imaging Spectroradiometer
MSG	Meteosat Second Generation
NERC	Natural Environment Research Council
NRT	Near real–time
OLR	Outgoing longwave radiation
PSF	Point spread function
RAL	Rutherford Appleton Laboratory
RMIB	Royal Meteorological Institute of Belgium
RSW	Reflected shortwave radiation
SEVIRI	Spinning Enhanced Visible and Infrared Imager
SINERGEE	Simulations from an NWP model to Exploit Radiation data from a Geostationary satellite, Explore radiative processes and evaluate models
SOL	Start of line
SW	Shortwave
TOA	Top of atmosphere
WVF	Water vapor feedback

REFERENCES

Allan, R. P., A. Slingo, S. Milton, and I. Culverwell, 2004: SINERGEE: Simulation and exploitation of data from Meteosat-8 using an NWP model. *Proc. EUMETSAT Meteorological Satellite Conf.,* Prague, Czech Republic, EUMETSAT, 121–129.

Allen, M. R., P. Stott, J. Mitchell, R. Schnur, and T. Delworth, 2000: Quantifying the uncertainty in forecasts of anthropogenic climate change. *Nature,* **407,** 617–620.

Bell, S., S. Milton, C. Wilson, and T. Davies, 2002: A new Unified Model. *NWP Gazette,* June 2002, 3–7.

Brindley, H. E., 2004: Estimation of the radiative effects of aerosol using GERB and SEVIRI. *Proc. EUMETSAT Meteorological Satellite Conf.,* Prague, Czech Republic, EUMETSAT, 512–517.

Charlson, R. J., S. E. Schwartz, J. M. Hales, R. D. Cess, J. A. Coakley Jr., J. E. Hansen, and D. J. Hoffman, 1992: Climate forcing by anthropogenic aerosols. *Science,* **255,** 423–430.

Clerbaux, N., S. Dewitte, L. Gonzalez, C. Bertrand, B. Nicula, and A. Ipe, 2003: Outgoing longwave flux estimation: Improvement of angular modelling using spectral information. *Remote Sens. Environ.,* **85,** 389–395.

Futyan, J. M. and J. E. Russell, 2005: Developing clear sky flux products for the Geostationary Earth Radiation Budget (GERB) experiment. *J. Appl. Meteor.,* in press.

——, ——, and J. E. Harries, 2004: Cloud radiative forcing in Pacific, African, and Atlantic tropical convective regions. *J. Climate,* **17,** 3192–3202.

——, ——, ——, 2005: Determining cloud forcing by cloud type from geostationary satellite data, *Geophys. Res. Lett.,* **32,** L08807, doi:10.1029/2004GL022275.

Gonzalez, L., A. Hermans, S. Dewitte, A. Ipe, G. Sadowski, and N. Clerbaux, 2000: Resolution enhancement of GERB data. *Proc. EUMETSAT Meteorological Satellite Data User's Conf.,* Bologna, Italy, EUMETSAT, 619–625.

Gueymard, C. A., 2004: The sun's total and spectral irradiance for solar energy applications and solar radiation models. *Sol. Energy,* **76**, 423–453.

Harries, J. E., 1997: Atmospheric radiation and atmospheric humidity. *Quart. J. Roy. Meteor. Soc.,* **123,** 2173–2186.

——, and D. Crommelynck, 1999: The Geostationary Earth Radiation Budget experiment on MSG-1 and its potential application. *Adv. Space Res.,* **24,** 915–919.

Harrison, E. F., P. Minnis, B. R. Barkstrom, V. Ramanathan, R. D. Cess, and G. G. Gibson, 1990: Seasonal variation of cloud radiative forcing derived from the Earth Radiation Budget Experiment. *J. Geophys. Res.,* **95,** 18 687–18 703.

Houghton, J. T., Y. Ding, D. J. Griggs, M. Noguer, P. J. van der Linden, X. Dai, K. Makskell, and C. A. Johnson, Eds., 2001: Climate Change 2001: The Scientific Basis. Cambridge University Press, 944 pp.

Ipe, A., N. Clerbaux, C. Bertrand, S. Dewitte, and L. Gonzalez, 2003: Pixel-scale composite top-of-the-atmosphere clear-sky reflectances for Meteosat-7 visible data. *J. Geophys. Res.,* **108** (D19), 4612, doi:10.1029/2002JD002771.

——, C. Bertrand, N. Clerbaux, S. Dewitte, and L. Gonzalez, 2004: Validation and homogenisation of cloud optical depth and cloud fraction retrievals for GERB/SEVIRI scene identification using Meteosat-7 data. *Atmos. Res.,* **72,** 17–37.

Kandel, R., and Coauthors, 1998: The ScaRaB Earth radiation budget dataset. *Bull. Amer. Meteor. Soc.,* **79,** 765–783.

Key, J., and A. J. Schweiger, 1998: Tools for atmospheric radiative transfer: Streamer and Fluxnet. *Comput. Geosci.,* **24,** 443–451.

Lindzen R. S., 1990: Some coolness concerning global warming. *Bull. Amer. Meteor. Soc.,* **71,** 288–299.

Loeb, N. G., N. M. Smith, S. Kato, W. F. Miller, S. K. Gupta, P. Minnis, and B. A. Wielicki, 2003: Angular distribution models for top-of-atmosphere radiative flux estimation from the Clouds and the Earth's Radiant Energy System instrument on the Tropical Rainfall Measuring Mission Satellite. Part I: Methodology. *J. Appl. Meteor.,* **42,** 240–265.

Minschwaner, K., and A. E. Dessler, 2004: Water vapor feedback in the tropical upper troposphere: Model results and observations, *J. Climate,* **17,** 1272–1282.

Mossavati, R., J. E. Harries, S. Kellock, R. T. Wrigley, J. Mueller, and N. P. Fox, 1998: Radiometric calibration of the GERB instrument. *Metrologia,* **35**, 603–607.

Munro, R., A. Ratier, J. Schmetz, and D. Klaes, 2002: Atmospheric measurements from the MSG and EPS systems. *Adv. Space Res.,* **29,** 1609–1618.

Nakajima, T., and M. D. King, 1990: Determination of the optical thickness and effective particle radius of clouds from reflected solar radiation measurements. Part I: Theory. *J. Atmos. Sci.,* **47,** 1878–1893.

Pope, V. D., M. Gallani, P. R. Rowntree, and R. A. Stratton, 2000: The impact of new physical parametrizations in the Hadley Centre climate model—HadAM3. *Climate Dyn.,* **16,** 123–146.

Ramanthan, V., R. D. Cess, E. F. Harrison, P. Minnis, B. R. Barkstrom, E. Ahmad, and D. Hartmann, 1989: Cloud-radiative forcing and climate: Results from the Earth Radiation Budget Experiment. *Science,* **243,** 57–62.

Rind D., E. W. Chiou, W. Chu, J. Larsen, S. Oltmans, J. Lerner, M. P. McCormick, and L. McMaster, 1991: Positive water-vapor feedback in climate models confirmed by satellite data. *Nature,* **349,** 500–503.

Ringer, M. A., J. M. Edwards, and A. Slingo, 2003: Simulation of satellite channel radiances in the Met Office Unified Model. *Quart. J. Roy. Meteor. Soc.,* **129,** 1169–1190.

Sandford, M. C. W.,and Coauthors, 2003: The geostationary Earth radiation budget (GERB) instrument on EUMETSAT's MSG satellite. *Acta Astron.,* **53,** 909–915.

Schmetz, J., P. Pili, S. Tjemkes, D. Just, J. Kerkmann, S. Rota, and A. Ratier, 2002: An introduction to Meteosat Second Generation (MSG). *Bull. Amer. Meteor. Soc.,* **83,** 977–994.

Senior, C. A., and J. F. B. Mitchell, 1993: CO^2 and climate: The impact of cloud parameterisation. *J. Climate,* **6,** 393–418.

Slingo, A., K. I. Hodges, and G. J. Robinson, 2004: Simulation of the diurnal cycle in a climate model and its evaluation using data from Meteosat 7. *Quart. J. Roy. Meteor. Soc.,* **130,** 1449–1467.

Smith, G. L., and Coauthors, 2003: Method for comparison of GERB and CERES radiances. *Proc. 10th Int. Symp. Remote Sensing,* Barcelona, Spain, Society of Photo-Optical Instrumentation Engineers, 5234.

Soden B. J., R. T. Wetherald, G. L. Stenchikov, and A. Robock, 2002: Global cooling after the eruption of Mount Pinatubo: A test of climate feedback by water vapor. *Science,* **296,** 727–730.

Stott, P. A., S. F. Tett, G. S. Jones, M. R. Allen, J. F. Mitchell, and G. J. Jenkins, 2000: External control of 20th century temperature by natural and anthropogenic forcings. *Science,* **290,** 2133–2137.

Washington R., M. Todd, N. J. Middleton, and A. S. Goudie, 2003: Dust-storm source areas determined by the Total Ozone Monitoring Spectrometer and surface observations, *Ann. Assoc. Amer. Geogr.,* **93,** 297–313.

Webb, M. J., C. A. Senior, S. Bony, and J.-J. Morcrette, 2001: Combining ERBE and ISCCP data to assess clouds in the Hadley Centre, ECMWF and LMD atmospheric models. *Climate Dyn.,* **17,** 905–922

Wielicki, B. A., and Coauthors, 2002: Evidence for large decadal variability in the tropical mean radiative energy budget. *Science,* **295,** 841–844.

Yang, G.-Y., and J. M. Slingo, 2001: The diurnal cycle in the Tropics. *Mon. Wea. Rev.,* **129,** 784–801.

Young, D. F., P. Minnis, D. R. Doelling, G. G. Gibson, and T. Wong, 1998: Temporal interpolation methods for the Clouds and the Earth's Radiant Energy System (CERES) Experiment. *J. Appl. Meteor.,* **37,** 572–590.